THE JOURNAL OF PHYSICAL CHEMISTRY C
A JOURNAL OF THE AMERICAN CHEMICAL SOCIETY

pubs.acs.org/JPCC

Article

Molecular-Level Insight into Charge Carrier Transport and Speciation in Solid Polymer Electrolytes by Chemically Tuning Both Polymer and Lithium Salt

Brigette A. Fortuin, Leire Meabe, Sergio Rodriguez Peña, Yan Zhang, Lixin Qiao, Julen Etxabe, Lorena Garcia, Hegoi Manzano, Michel Armand, María Martínez-Ibañez,* and Javier Carrasco*

Cite This: J. Phys. Chem. C 2023, 127, 1955−1964

Read Online

ACCESS | Metrics & More | Article Recommendations | Supporting Information

ABSTRACT: The advent of Li-metal batteries has seen progress toward studies focused on the chemical modification of solid polymer electrolytes, involving tuning either polymer or Li salt properties to enhance the overall cell performance. This study encompasses chemically modifying simultaneously both polymer matrix and lithium salt by assessing ion coordination environments, ion transport mechanisms, and molecular speciation. First, commercially used lithium bis(trifluoromethanesulfonyl)imide (LiTFSI) salt is taken as a reference, where F atoms become partially substituted by one or two H atoms in the $-CF_3$ moieties of LiTFSI. These substitutions lead to the formation of lithium-(difluoromethanesulfonyl)(trifluoromethanesulfonyl)imide (LiDFTFSI) and lithium bis(difluoromethanesulfonyl)imide (LiDFSI) salts. Both lithium salts promote anion immobilization and increase the lithium transference number. Second, we show that exchanging archetypal poly(ethylene oxide) (PEO) with poly(ε-caprolactone) (PCL) significantly changes charge carrier speciation. Studying the ionic structures of these polymer/Li salt combinations (LiTFSI, LiDFTFSI or LiDFSI with PEO or PCL) by combining molecular dynamics simulations and a range of experimental techniques, we provide atomistic insights to understand the solvation structure and synergistic effects that impact macroscopic properties, such as Li^+ conductivity and transference number.

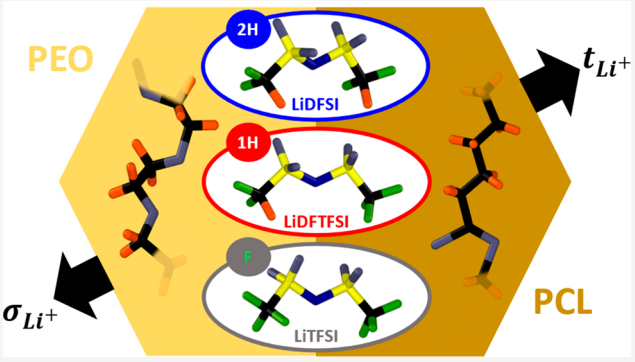

1. INTRODUCTION

The revival of all-solid-state lithium metal batteries (ASSLMBs) plays a vital role in electrical energy storage and supply as the market continues to mature toward electric vehicles, mobile devices, and stationary storage systems. This increasing demand for higher energy density batteries is limited by current lithium-ion battery (LIB) technology, which requires active materials with higher capacity and, concurrently, avoidance of unsafe, flammable organic solvents.[1−3]

Solid polymer electrolytes (SPEs), a solvent-free salt solution in a polymer host, are a particularly strong class of electrolytes for the implementation of ASSLMBs, considering their ease of processability, flexibility, low cost, longer cycle life, and improved safety,[4−8] compared to typically used carbonate-based liquid solutions as an electrolyte in LIBs.[2,3,9] However, the low Li^+ conductivity, slower transport mechanism, and compromised stability at high voltages of SPEs are some of the characteristics that hinder their application toward ASSLMBs, making a better fundamental understanding of these materials, down to the atomistic level, indispensable.

Poly(ethylene oxide) (PEO) combined with lithium salts has been the workhorse system for SPEs development in recent years, since first proposed by Armand.[10] PEO enables high ionic conductivity at temperatures above 60 °C (10^{-4} S cm^{-1}), but the facile oxidation of the C−O−C bonds limits its anodic stability. Additionally, the strong interaction between Li^+ ions and the ethylene oxide (EO) units of PEO results in high Li salt dissociation and a low lithium transference number (t_{Li^+}) of 0.2 when employing lithium bis(trifluoromethanesulfonyl)imide (LiTFSI).[11−13] The lower lithium mobility is observed due to the chelating effect of the EO units which form a crown ether with lithium ions, arising from the oxygen dense structure and the strong ion-dipole interaction between ether oxygens and lithium.[14,15] In turn, this generates detrimental anion concentration gradients during battery operation. Hence, the search for alternative polymers is imperative.

Received: October 5, 2022
Revised: January 9, 2023
Published: January 24, 2023

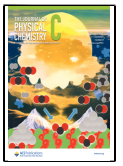

Carbonyl-coordinating polymers, primarily aliphatic polycarbonates and polyesters, are a promising alternative due to higher t_{Li^+} resulting from interactions between the polymer and the anion from the Li salt[16] and a wide electrochemical stability.[12,17−19] Of particular interest is poly(ε-caprolactone) (PCL) due to the attainment of a higher t_{Li^+} of 0.4 with LiTFSI,[12,17] as weaker lithium cation coordination with carbonyl-based polymers transpires, resulting in a higher lithium mobility. Comparing PCL to broadly studied PEO, the chelating effect of the EO units changes the coordination structure and influences the ionic transport mechanism.[14] By replacing PEO with PCL, a deeper understanding of the different ionic species and types of ionic interactions, such as polymer−ion, polymer−polymer, and ion−ion interaction interdependencies, termed molecular speciation, may provide insights into the ion transport mechanisms of these distinctly different polymer chemistries.

Among all of the studied lithium salts, LiTFSI has garnered significant interest toward the realization of commercial solid-state batteries because of its thermal and chemical stability, structural flexibility, and amorphization effect when incorporated with PEO as a host matrix.[8,11,12,20−24] Recently, alternative imide lithium salts have been designed, for example, by replacing the F atom with a H atom, on one or both $-CF_3$ groups, obtaining lithium(difluoromethanesulfonyl)(trifluoromethanesulfonyl)imide (LiDFTFSI) or lithium bis(difluoromethanesulfonyl)imide (LiDFSI), respectively, as we have investigated in recent studies.[11,23−25] The replacement of electron-withdrawing F atom(s) with electron-donating H atom(s), i.e., weakly acidic $-CF_2H$ groups, induces a facile decomposition of LiDFTFSI and LiDFSI against a Li^0 anode. This leads to the formation of several favorable solid electrolyte interphase (SEI) species, namely mechanically stable lithium fluoride (LiF) and ionically conductive lithium hydride (LiH), promoting longer cycling performance.[11,23] With regard to ionic transport, the presence of acidic H atom(s) enables noncovalent weak hydrogen bond interactions between the Li salt and the Lewis basic O atom from the polymer, resulting in stronger polymer−anion interactions that dwindles anionic mobility and, therefore increases the t_{Li^+} and Li^+ ionic conductivity, in addition to decreasing concentration gradients upon cycling.[11,23]

Despite these important findings, an accurate fundamental understanding of ionic transport phenomena and charge carrier speciation in this class of SPEs is broadly lacking and urgently needed. Insights into these aspects should provide guidance to tune the behavior of SPEs under electrochemical operation through rational chemical modification of their components, ultimately yielding new design strategies to improve their performance. Herein, we tackle these related issues by simultaneously modifying the chemistries of both polymer host and lithium salt and performing a deep analysis that combines theory and experiments.

Six SPE systems have been considered utilizing both polymers (PEO or PCL) combined with each of the lithium salts (LiTFSI, LiDFTFSI, or LiDFSI). Following previous studies, the Li salt concentration has been adjusted for each considered polymer host to maximize the ionic conductivity and overall performance.[26,27] EO/Li (CL/Li) ratios of 16 (6) for PEO(PCL)-SPEs are utilized, corresponding to approximately 30 wt % of lithium salt for each system. Optimal ionic conductivity for PEO systems is achieved at EO/Li ratios of 12−16, with optimal mechanical properties achieved at an EO/Li ratio of 20.[26,28] For PCL, a more concentrated system is required to curtail chain stacking and crystallinity, enabling increased Li^+ diffusion and, hence, a CL/Li ratio of 6.[29]

For all the investigated systems, upon the determination of their thermal properties using differential scanning calorimetry (DSC) and electrochemical properties using electrochemical impedance spectroscopy (EIS), we use Raman spectroscopy to analyze ion coordination and local interactions. Further insights into charge carrier speciation are gained via classical molecular dynamics (MD) simulations.

2. EXPERIMENTAL AND THEORETICAL METHODS

2.1. Materials. Poly(ethylene oxide) (PEO, $M_w = 5 \times 10^6$ g mol^{-1}), poly(ε-caprolactone) (PCL, $M_w = 8 \times 10^4$ g mol^{-1}), tetrahydrofuran (THF), acetonitrile (ACN), and lithium bis(trifluoromethane)sulfonimide (LiTFSI) (99.9%) were purchased from Sigma-Aldrich. The novel salts, lithium (difluoromethanesulfonyl)(trifluoromethanesulfonyl)imide (LiDFTFSI) and lithium bis(difluoromethanesulfonyl)imide (LiDFSI), were synthesized following the synthesis procedures reported by Zhang et al.[24,30] and Qiao et al.,[11] respectively. LiTFSI, LiDFTFSI, and LiDFSI salts were dried overnight at 100 °C under vacuum prior to use. All the procedures related to the moisture- or oxygen-sensitive materials were performed in an argon-filled glovebox (MBraun, H_2O and O_2 < 0.5 ppm).

2.2. Preparation of Polymer Electrolyte Membranes. Six SPE formulations based on EO/Li = 16 and CL/Li = 6 for PEO and PCL, respectively, were prepared with each of the lithium salts: LiTFSI, LiDFTFSI, and LiDFSI. The conventional solvent-casting method was used, followed by a two-step drying process of 24 h under ventilation at 35 °C, followed by 24 h under vacuum at 50 °C, to ensure the removal of any traces of solvent. The PEO systems were dissolved using acetonitrile, and PCL systems were dissolved using tetrahydrofuran. Hot pressing produced SPEs with varying thicknesses, with PEO (60 °C, 3 tons, 50 s) and PCL (50 °C, 2 tons, 30 s). SPEs with a thickness and diameter of 300 μm and 4 mm, respectively, were hot pressed for ionic conductivity measurements as well as 100 μm and 16 mm, respectively, for lithium symmetric cell measurements.

2.3. Differential Scanning Calorimetry. The phase transition behavior of the SPEs were studied using a DSC Discovery 2500 (TA Instruments) from −80 to 100 °C with heating and cooling rates of 10 K min^{-1}. Samples (ca. 10 mg) were sealed in Al crucibles in an argon-filled glovebox. The second heating scan was used to determine the values for the glass transition temperature (T_g, onset of the heat capacity change), melting temperature (T_m, the maximum of the endothermic peak) and melting enthalpy (ΔH_m, the area below the endothermic peak). The crystalline fraction (χ_c) of the polymer electrolytes was calculated by eq 1 below:

$$\chi_c = \frac{\Delta H_m}{\Delta H_{PEO/PCL} f_{PEO/PCL}} \times 100\% \quad (1)$$

where ΔH_m is the melting enthalpy of the electrolyte and $\Delta H_{PEO/PCL}$ is the melting enthalpy for 100% crystalline polymer matrix, where the values are 205 and 139.5 J g^{-1} for PEO and PCL, respectively, as reported in the literature,[12] and $f_{PEO/PCL}$ is the polymer weight fraction in the electrolyte.

2.4. Ionic Conductivity and Lithium Transport Number. Both ionic conductivity and Li-ion transport number were measured in CR2032 type coin cells. All cells were

https://doi.org/10.1021/acs.jpcc.2c07032
J. Phys. Chem. C 2023, 127, 1955−1964

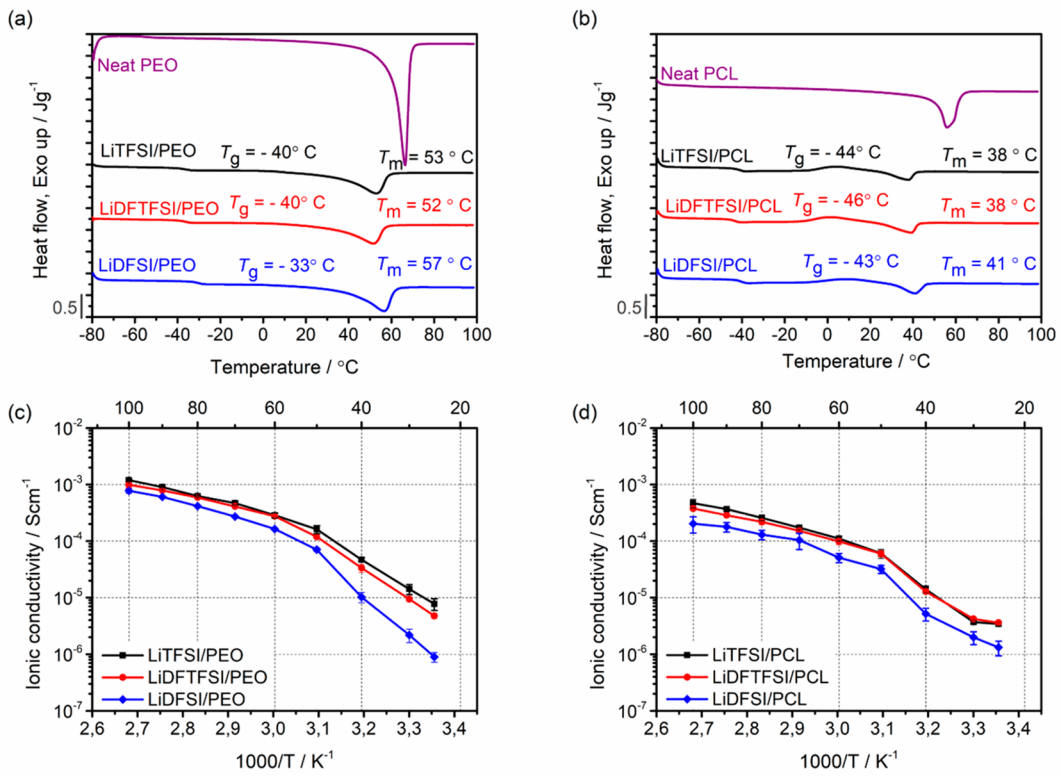

Figure 1. DSC traces of (a) PEO- and (b) PCL-based SPEs. DSC scan recorded during the second heating at 10 K min^{-1}. Temperature dependence of the ionic conductivity for (c) PEO- and (d) PCL-based SPEs based on EIS. Neat polymers are indicated in purple, LiTFSI-based SPEs in black, LiDFTFSI-based SPEs in red, and LiDFSI-based SPEs in blue. The error bars for (c) and (d) are based on at least 3 samples per studied system.

assembled in an argon-filled glovebox. For ionic conductivity, two stainless steel (SS) blocking electrodes were used, with the configuration SS|SPE|SS and with an SPE area of 0.1257 cm^2. The measurement was performed by EIS using a Multichannel VMP3 (Biologic, Claix, France) with a signal amplitude of 20 mV for PEO and 100 mV for PCL over the frequency range 10^{-1}−10^6 Hz, at 25 °C and with 10 °C intervals from and including 30 to 100 °C. A period of 1 h was employed as a stabilization between different measurements. The ionic conductivity is calculated using eq 2:

$$\sigma_{DC} = \frac{t}{R_{bulk}A} \tag{2}$$

where t is the thickness of the electrolyte (ca. 0.3 mm), A represents the area of the electrolyte, which is 0.1257 cm^2, and R_{bulk} represents the bulk resistance of the polymer electrolyte measured by EIS.

Li-symmetric cells were assembled with the Li|SPE|Li configuration and with a Li-metal area of 0.5026 cm^2. The Li-ion transport number was measured following the procedures at 70 °C, as described by Hu's method.[31] The electrolytes were sandwiched between two lithium discs in CR2032 type coin cells. Before the analysis, the cells were left to stabilize at 70 °C for 6 h. The Li-ion transport number was calculated according to eq 3:

$$t_{Li^+} = \frac{R_{cell}}{\Delta V / I_{SS}} \tag{3}$$

where t_{Li^+} represents the Li-ion transport number, R_{cell} is the initial cell resistance consisting of the sum of the bulk and interfacial resistance, ΔV represents the total polarization voltage, and I_{SS} is the steady-state current.

2.5. Raman Spectroscopy. Raman spectra were collected at room temperature using a Renishaw inVia confocal Raman spectrometer (serial number 16H981) using an incident laser with a wavelength of 532 nm (laser spot size: 0.8 μm; spatial resolution: ∼0.4 μm). Contamination from ambient atmosphere (e.g., air and water) was avoided by placing the samples in a sealed, airtight cell built with a Raman-inactive glass window which was assembled in an argon-filled glovebox. The Raman spectra were collected in the range of 3000−300 cm^{-1} Raman shift.

2.6. Theoretical Methods and Computational Details. Classical MD simulations were conducted on LiTFSI/PEO, LiDFTFSI/PEO, and LiDFSI/PEO with an EO/Li ratio of 16:1 and on LiTFSI/PCL, LiDFTFSI/PCL, and LiDFSI/PCL with a CL/Li ratio of 6:1 using Gromacs.[32] The simulation boxes of LiTFSI/PEO, LiDFTFSI/PEO, and LiDFSI/PEO consisted of 40 PEO chains with 24 EO repeating units in each chain and 60 LiTFSI, LiDFTFSI, and LiDFSI ion pairs, respectively. In the case of LiTFSI/PCL, LiDFTFSI/PCL, and LiDFSI/PCL, the simulation boxes consisted of 20 PCL chains with 24 CL repeating units in each chain and 80 LiTFSI, LiDFTFSI, and LiDFSI ion pairs, respectively. The initial boxes were generated directly with Gromacs, placing each molecule randomly in a larger simulation box with a low density, for all cases.

First, the structures were compressed at 10 K with a pressure of 98.99 atm (100 bar) to reach densities closer to the experiments using the Berendsen thermostat and the

https://doi.org/10.1021/acs.jpcc.2c07032
J. Phys. Chem. C 2023, 127, 1955−1964

Parrinello−Rahman barostat (a relaxation time was 5 ps for all cases). Following this, the systems were gradually heated to 600 K at 1 atm and equilibrated at this temperature in a NVT ensemble to break possible metastable configurations. The systems were then cooled to the simulation temperature of 343 K (70 °C) at 1 atm. The final configuration was further equilibrated during 1 ns at the same temperature and pressure. The production simulation was performed for 200 ns in the NVT ensemble to ensure that the system reached a diffusive regime. The energy potentials of PEO, PCL, Li^+, $TFSI^-$, $DFTFSI^-$, and $DFSI^-$ were described by the all-atom optimized potentials for liquid simulations (OPLS-AA) force field.[33−38] The force field parameters (bond, angle, torsion angle, and Lennard-Jones potential) for PEO, PCL, Li^+, $TFSI^-$, $DFTFSI^-$, and $DFSI^-$ were taken from the OPLS-AA force field.

The structures of the anions ($TFSI^-$, $DFTFSI^-$, and $DFSI^-$) were optimized at density functional theory (DFT) level with the Fritz Haber Institute ab initio molecular simulations (FHI-aims) software.[39,40] The Becke's three parameters (B3) exchange functional together with the Lee−Yang−Parr (LYP) nonlocal correlation functional (B3LYP)[41,42] was adopted with the "tier2" standard basis set in the FHI-aims code. DFT (FHI-AIMS) was used to calculate the partial atomic charges required for the MD simulations using the electrostatic potential (ESP) method. The Li^+ charge was reduced to +0.7 to equal the scale factor applied to $TFSI^-$ and to keep the system neutrally charged.[11,12,43−48] The cutoff for van der Waals force and the real space of Ewald summation was 10 Å. The fast smooth particle mesh Ewald (PME) electrostatics was used to treat Coulomb interactions in a periodic system.

3. RESULTS AND DISCUSSION

3.1. Thermal Characterization. The crystalline−amorphous phase transitions of the investigated SPEs were evaluated first, which is closely related to the flexibility of the polymer chains and transport properties, thus dictating the overall performance.

The DSC traces provided in Figure 1a for PEO-based SPEs show similar T_g for LiTFSI/PEO and LiDFTFSI/PEO, with LiDFSI/PEO possessing the highest T_g (Figure 1a and Table S1). The presence of two "acidic" hydrogens in LiDFSI may increase long-range interactions between $DFSI^-$ and PEO, requiring additional energy to undergo the transition from glassy to rubbery state, thereby raising its T_g to −33 °C. This effect may be expected for LiDFTFSI/PEO;[24,30] however, both LiDFTFSI/PEO and LiTFSI/PEO follow similar glass transitions, at −40 °C. Focusing now on the T_m, asymmetrical LiDFTFSI produces the lowest T_m for LiDFTFSI/PEO with 52 °C compared to LiTFSI/PEO with a T_m of 53 °C. The introduction of two $-CF_2H$ moieties in LiDFSI/PEO yields a slightly higher T_m of 57 °C, attributed to the hampered dissociation of Li^+ cations from sulfonimide anions, resulting in a higher enthalpy of melting (Table S1), as shown in our previous work.[11,24,30] The hindered dissociation presents a lower amorphization ability for LiDFSI salt in PEO matrix and renders a higher T_m and higher crystallinity degree (Table S1). Because the differences in the thermal properties are not significantly large, the effect of modifying the Li salts in PEO is comparable, possibly due to the good solvating capabilities of PEO and the similar structural flexibility of these lithium salts.[11,24] Upon interchanging PEO with PCL, a different trend in the T_g is observed, as LiDFTFSI/PCL now exhibits a slightly lower T_g of −46 °C, with LiTFSI/PCL and LiDFSI/PCL possessing similar T_g values of −44 and −43 °C, respectively (Figure 1b and Table S2). The phase transition from ordered to disordered PCL-based SPEs occurs at a slightly lower T_m for LiTFSI/PCL and LiDFTFSI/PCL, 38 °C, compared to LiDFSI/PCL, 41 °C, yet overall remain comparable regarding thermal properties (Table S2).

Overall, despite the slightly higher concentration of lithium salt (∼0.5%) within the PCL-based system compared to PEO-based SPEs, the impact on the thermal properties of these systems for the respective polymer matrices is similar regardless of the Li salt chemistry; however, in the case of PEO, stronger Li^+ coordination with the EO units allows for higher ionic dissociation and, therefore higher enthalpies of melting (Tables S1 and S2). Additionally, the degree of crystallinity, χ_c, significantly reduces upon the introduction of the lithium salts into the respective polymer host matrices, displaying good amorphization effects in both cases.[11,12,23−25]

Previously reported PEO systems based on these Li salts[11,21−23,28] exhibit similar thermal properties as shown in Figure 1a, hypothesizing the presence of the additional interactions upon the introduction of H atom(s), which may affect ion transport properties. The investigation of LiTFSI in PEO, PCL, and polymer blends by Meabe et al.[12] distinctly demonstrates the lower dissociation of LiTFSI in PCL compared to PEO, as well as the lower T_g of LiTFSI/PCL which is linked to better segmental motion. Hence, it is evident that a different solvation mechanism dominates in PEO- compared to PCL-based SPEs.

3.2. Ion Transport. The temperature dependence of the total ionic conductivity (σ_{total}) was measured by EIS (Figure 1c,d), revealing comparable σ_{total} for LiTFSI/PEO and LiDFTFSI/PEO and slightly lower σ_{total} for LiDFSI/PEO, as evidenced by the thermal properties (Table S1). The σ_{total} for PCL-based SPEs follows a similar trend.

Focusing on the effect of the polymer host, the slightly higher σ_{total} displayed for PEO-based as opposed to PCL-based SPEs, regardless of the salt chemistry, is ascribed to the higher Li salt dissociation ability of PEO,[12,14] solvating lithium cations in a crown ether conformation.[12,20] Albeit PCL-based SPEs display an overall higher polymer segmental motion, depicted by its lower T_g values, its σ_{total} is generally lower compared to PEO-based SPEs (Figure 1c,d). Considering that the ion transport properties are highly influenced by the segmental motion of the polymer matrix, it is not the only factor that affects the ionic conductivity because it has been reported that PEO has a stronger solvating ability of lithium salts[11,24] compared to other types of polymer matrices, such as PCL; PEO-based matrices are observed to possess higher σ_{total}. Additionally, a sudden conductivity decrease observed at temperatures below 50 °C is attributed to the semicrystalline nature of both PEO- and PCL-based SPEs, restricting the mobility of the polymer chains and hindering the diffusion of the ions below this temperature.[11,12]

Upon modifying the Li salt chemistry, LiDFSI-based SPEs displays the lowest σ_{total}, ascribed to a 3-fold effect: (1) a lower dissociation degree of LiDFSI compared to LiDFTFSI and LiTFSI because of the lower electron-withdrawing ability of $-CF_2H$ moieties, resulting in stronger Li^+−anion interactions;[23,30] (2) greater probability of producing H-bonding interactions between $DFSI^-$ anions and PEO;[11,30] and (3) hindered diffusion of the ionic species due to polymer chain

https://doi.org/10.1021/acs.jpcc.2c07032
J. Phys. Chem. C 2023, 127, 1955−1964

mobility restriction, as depicted by higher T_g, T_m, and χ_c value in Figures 1a,b as well as Tables S1 and S2.

A key ionic transport property of SPEs describing the efficiency of ion transport may provide greater insights regarding the ion transport mechanisms within the respective polymer matrices. The lithium transference number (t_{Li^+}) is deduced from the specific conductivity of Li^+ ions (σ_{Li^+}) and is displayed in Figure 2 for all the studied systems at 70 °C.

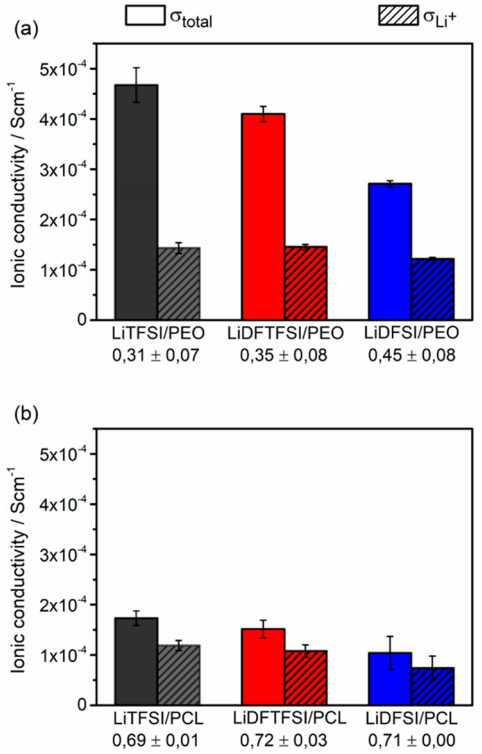

Figure 2. Histogram illustrating the total (full color) and Li^+ (striped) ionic conductivity with error bars at 70 °C of (a) PEO- and (b) PCL-based SPEs as a function of the studied lithium salt. LiTFSI-based SPEs are shown in black, LiDFTFSI-based SPEs in red, and LiDFSI-based SPEs in blue. The error bars are based on at least 3 samples per studied system.

The proposed ion transport mechanism in the PEO matrix follows lithium ions coordinated by 3−5 EO units facilitating "lithium ion hopping" from one coordination site to another, either intrachain or interchain.[12,15,26,49] PEO-based SPEs undergo a systematic increase of t_{Li^+} upon increasing the H content of the anion, tabulated in Table S3 (t_{Li^+} = 0.31, 0.35, and 0.45 for LiTFSI/PEO, LiDFTFSI/PEO, and LiDFSI/PEO, respectively), indicating that the lithium salts consequently undergo an anionic mobility restriction with increasing H content in PEO.[11,23,24,30] Interestingly, this effect is seemingly absent in PCL-SPEs (Figure 2b and Table S3), with nearly constant t_{Li^+} values (~0.7) when changing the lithium salt, suggesting the existence of more complex charge carrier speciation in PCL matrices as well as subtle polymer−ion, polymer−polymer, and ion−ion interaction interdependencies in these systems, as we shall examine more in depth later.

To further understand the role of local interactions, ion coordination, and speciation in the behavior of the studied SPEs, Raman spectroscopy was combined with MD simulations as discussed in the following sections.

3.3. Raman Spectroscopic Analyses. Elucidation of the extent of ion dissociation, ion coordination, and consequently greater insight into the ionic speciation types of the studied SPE systems were aided with Raman spectroscopy.

Centralizing on the Raman spectra of the neat lithium salts in Figure 3a, LiTFSI is observed in associated form via the S−N−S vibrational mode at 747 cm^{-1}.[12,20,28,50] Introducing an H atom, LiDFTFSI shifts down slightly to 745 cm^{-1}. Intriguingly, when two H atoms are present in the form of $-CF_2H$ moieties for LiDFSI, the S−N−S vibrational mode undergoes a significant red-shift to a lower wavenumber of 703 cm^{-1}. The downshift to lower wavenumbers for LiDFTFSI and LiDFSI may be assigned to the lower bond strength of C−H bonds compared to C−F bonds, 415 vs 439 kJ mol^{-1}, decreasing the force constant and thereby decreasing the wavenumber.

The Raman spectra of LiTFSI-based SPEs are shown in Figure 3b, with results similar as found in the literature for both LiTFSI/PEO[12,28,50,51] and LiTFSI/PCL,[12,17] concluding that complete dissociation of LiTFSI occurs in PEO and partial dissociation occurs in PCL.[12] Interestingly, when it comes to LiDFTFSI-SPEs, illustrated in Figure 3c, the S−N−S vibration is observed to undergo a slight upshift from associated LiDFTFSI at 745 to 748 cm^{-1} for both LiDFTFSI/PEO and LiDFTFSI/PCL, with an additional peak observed at 717 cm^{-1} for LiDFTFSI/PCL. LiDFSI-based SPEs undergoes a similar upshift (Figure 3d), where associated LiDFSI is observed 707 cm^{-1}, while both LiDFSI/PEO and LiDFSI/PCL undergo a blue-shift to higher wavenumbers of 760 and 756 cm^{-1}, respectively. Once again, two distinct peaks are observed for the LiDFSI/PCL at 710 cm^{-1}. Both LiDFTFSI- and LiDFSI-based SPEs are found to encounter a blue-shift in both PEO and PCL polymer matrices, and in the case of PCL-based SPEs, both LiDFTFSI/PCL and LiDFSI/PCL exhibit two distinct peaks.

Because the Raman signal is influenced by the polarizability of a molecule, the concentration of loosely held electrons in the S−N−S bond results in large polarizability; consequently, the molecule will possess an intense Raman signal. From Figure 3a, the Raman peak for neat lithium salts decreases in intensity as the number of H atom(s) increases, which is correlated to the lower concentration of loosely held electrons around this bond, as $-CF_3$ moieties contain particularly higher electron density compared to $-CF_2H$ moieties. This is also the case for PCL-based SPEs, as the peak intensity for LiTFSI/PCL (Figure 3b) is higher compared to hydrogen-rich LiDFTFSI/PCL and LiDFSI/PCL, shown in Figure 3c,d.

What makes the spectral analysis particularly challenging to explain is how the presence of the H atom significantly changes the ionic speciation and ion coordination in either PEO or PCL matrices and, additionally, how the different polymer chemistries contribute to further changes in molecular speciation.

3.4. Molecular Speciation Utilizing Molecular Dynamics. After ionic coordination analysis by Raman spectroscopy, the full impact of the nature of the polymers and lithium salts under consideration on charge carrier speciation remains unsolved. Therefore, MD simulations are employed to gain such molecular-level understanding, regarding the different ionic species and types of ionic interactions, such as polymer−ion, polymer−polymer, and ion−ion interaction interdependencies, termed molecular speciation.

https://doi.org/10.1021/acs.jpcc.2c07032
J. Phys. Chem. C 2023, 127, 1955−1964

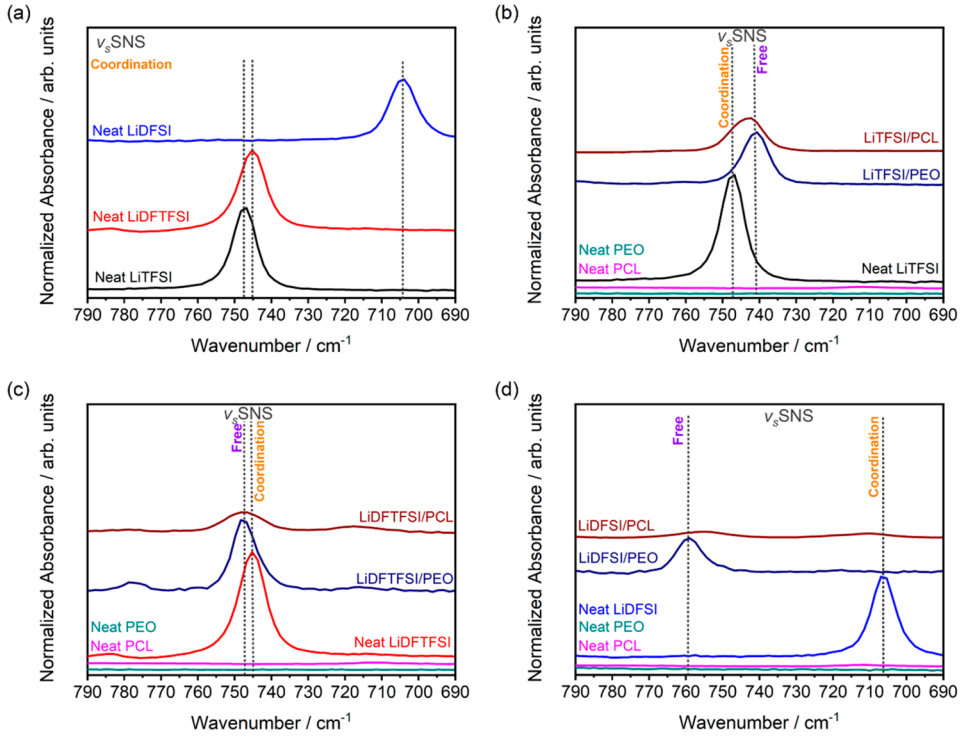

Figure 3. Raman spectra of (a) neat lithium salts, (b) LiTFSI-, (c) LiDFTFSI-, and (d) LiDFSI-based SPEs; representing LiTFSI (black), LiDFTFSI (red), LiDFSI (blue), neat PEO (cyan), PEO-based SPEs (navy), neat PCL (magenta), and PCL-based SPEs (dark red). The vertical dotted lines indicate the studied bonds as well as their vibration and coordination type.

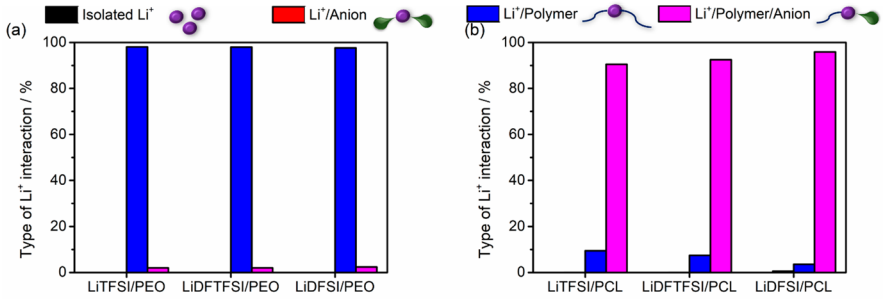

Figure 4. Molecular speciation analysis for Li^+ coordination in (a) PEO- and (b) PCL-based SPEs. The vertical bars consist of different colors which represent different types of molecular speciation, as shown in the legends above the respective figures.

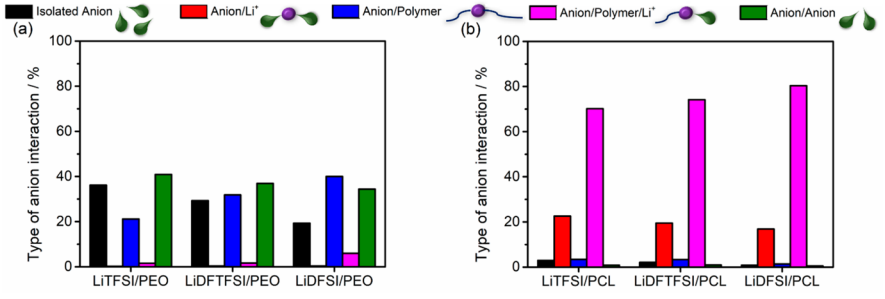

Figure 5. Molecular speciation analysis for anion coordination for (a) PEO- and (b) PCL-based SPEs. The vertical bars consist of different colors which represent different types of molecular speciation, as shown in the legends above the respective figures.

Radial distribution functions (RDFs) and coordination numbers (CNs) are computed to elucidate Li^+ coordination environments. The position and intensity of each RDF peak provide precise information about interaction distances between selected species and association degrees of such interactions, respectively. CNs can also be simply extracted from RDF analysis by integrating the area under the peaks of interest. Figure S1 shows all the computed RDFs considered in this work for the following discussions. Further speciation analysis is conducted on the Li^+ and anion coordination

https://doi.org/10.1021/acs.jpcc.2c07032
J. Phys. Chem. C 2023, 127, 1955−1964

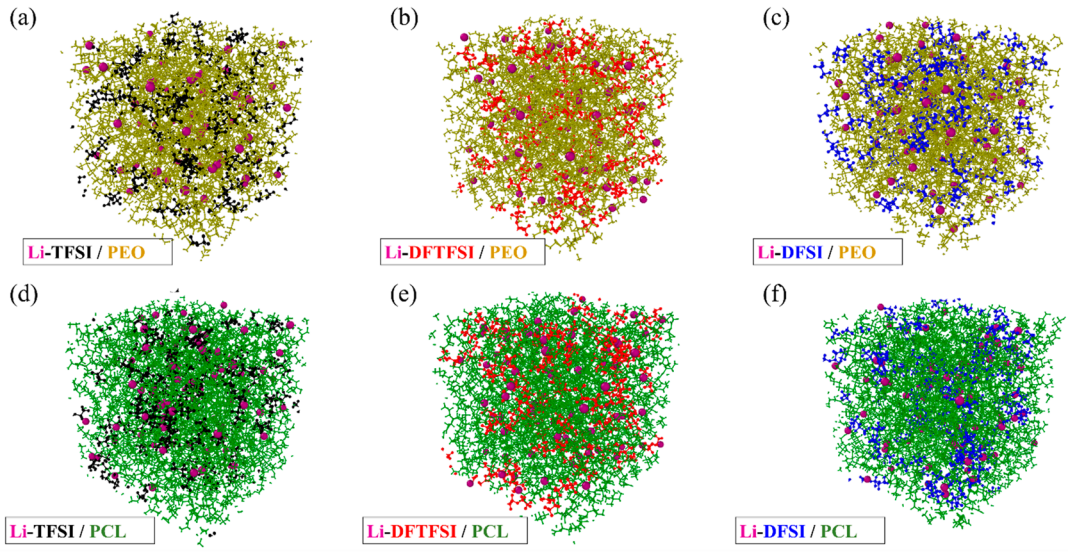

Figure 6. Molecular-level snapshots of MD simulations of (a) LiTFSI/PEO, (b) LiDFTFSI/PEO, (c) LiDFSI/PEO, (d) LiTFSI/PCL, (e) LiDFTFSI/PCL, and (f) LiDFSI/PCL at 70 °C. Li^+ is represented by purple balls; $TFSI^-$ (black), $DFTFSI^-$ (red) and $DFTFSI^-$ (blue) by stick models; and PEO (yellow) and PCL (green) by stick models within a coordination of 3 Å. The system name is labeled below each snapshot. Notice how in PEO-based SPEs (a–c) the lithium salts are more dissociated and mixed compared to PCL-based SPES (d–f).

environments to determine the mobility and extent of ion clustering on each investigated SPE (Figures 4 and 5). This mainly involves statistically tracking the fluctuating population of different isolated and interacting species (Li^+, anions, ion pairs, etc.) along the computed MD trajectories.

The RDFs for the interaction between Li^+ and the O atoms of the EO units in PEO ($Li-O_{PEO}^{C-O}$) are shown in Figure S1a, revealing a CN ≈ 5 independently of the considered lithium salt. In contrast, the interaction between Li^+ and the O atoms of the respective anions ($Li-O_{Anion}$) is almost nil (Figure S1c). Both $Li-O_{PEO}^{C-O}$ and $Li-O_{Anion}$ RDFs corroborate that complete Li salt dissociation occurs within all the PEO-based SPEs.[12,43−45,47,50] Yet, for PEO-based SPEs, RDF analysis conveys a similar degree of association for the lithium−PEO interaction ($Li-O_{PEO}^{C-O}$) upon changing the anionic structure, in contrast to the observed experimental trends regarding the different values measured for the lithium transference number (Figure 2a). The situation is very different in PCL (Figure S1b−d), where Li^+ preferentially interacts with the configuration $Li-O_{PCL}^{C=O}$, as reported in the literature[12] and confirmed by the computed RDFs. The highest $Li-O_{PCL}^{C=O}$ association occurs for both LiTFSI/PCL and LiDFTFSI/PCL, closely followed by LiDFSI/PCL, shown in Figure S1b. Accordingly, these results correlate well with the t_{Li^+} trend from Figure 2b. Additionally, the CN ≈ 3 for both $Li-O_{PCL}^{C=O}$ and $Li-O_{Anion}$ (Figure S1b−d) reveal formation of Li^+−anion pairs in PCL-based SPEs, in contrast to complete salt dissociation observed in PEO-based SPEs. These results explain the lowest σ_{total} measured for the LiDFSI/PCL SPE, as $DFSI^-$ anions are associated with Li^+ to a greater extent compared to the other studied lithium salts.

The molecular speciation analysis for each of the investigated SPEs is computed as the percentage of each type of isolated ions, ion aggregates, and other coordination structures that involve the polymer, with either lithium (Figure 4) or the respective anions (Figure 5) as the reference ionic species. A cutoff distance of 3 Å was selected based on the RDF analyses for lithium−polymer interactions: $Li-O_{PEO}^{C-O}$ and $Li-O_{PCL}^{C=O}$ (Figure S1a,b), where the first peak minimum is observed at this distance. A similar cutoff distance was selected for anion coordination to remain consistent, even though no first minimum is detected from the RDFs in Figure S1c,d.

As found from RDF analysis, for all studied PEO-based SPEs, Li^+ ions are essentially solvated by PEO, Li^+/Polymer (blue, Figure 4a), with the presence also of a small percentage (~2%) of coordination structures around Li^+ ions that, in addition to the EO units of the polymer, include the anion, Li^+/Polymer/Anion (magenta, Figure 4a), also tabulated in Table S4. When examining the anion coordination environment, we find that in PEO-based systems most of the anionic species ($TFSI^-$ and $DFTFSI^-$) tend to be noninteracting anion aggregates, Anion/Anion (green) (Figure 5a and Table S5), especially as the H content in the anion is increased. These noninteracting anion aggregates are defined as anion species in close range with one another considering a cutoff distance of 3 Å. However, when two H atoms are present, speciation changes in the case for $DFSI^-$ to mainly anion aggregates with polymer coordination, Anion/Polymer (blue). This finding is relevant, as the sum of both noninteracting Anion/Anion and interacting Anion/Polymer speciation increases as the number of H atom(s) increases (62% for LiTFSI/PEO, 69% for LiDFTFSI/PEO, and 74% for LiDFSI/PEO). These interactions, especially Anion/Polymer speciation, hinder anionic mobility and, hence, hinder anionic conductivity and explain the observed drop of σ_{total} (while increasing t_{Li^+}) when increasing the H content in the anion (Figure 2a). Notice how $DFSI^-$ anions undergo greater mobility restriction compared to $DFTFSI^-$ and $TFSI^-$, as the percentage of isolated $DFSI^-$ anions is the lowest, shown in Figure 5a (black) and Table S5. Similarly, as LiTFSI/PEO possesses the greatest degree of mobile isolated anions, this SPE exhibits the highest σ_{total}.

Intriguingly, we find that in PCL-based SPEs, polymer−anion assisted Li^+ coordination environment, Li^+/Polymer/Anion (magenta), is predominant (Figure 4b and Table S4), irrespective of the anionic species, and is especially high in the

https://doi.org/10.1021/acs.jpcc.2c07032
J. Phys. Chem. C 2023, 127, 1955−1964

case of LiDFSI/PCL (96%). When considering the t_{Li^+} from EIS measurements, where the most mobile Li^+ is observed in LiDFSI/PCL, as well as RDF analyses where the lowest Li−$O_{PCL}^{C=O}$ coordination is exhibited for this system, the speciation analysis qualitatively supports these results. Notably, anionic speciation analysis reveals an increase in polymer−Li^+ assisted anion coordination, Anion/Polymer/Li^+ speciation (magenta), in PCL matrices; from LiTFSI, LiDFTFSI, to LiDFSI and, when comparing these results to the σ_{total} based on EIS measurements, a decrease in anionic mobility is observed following a similar trend. Moreover, the anionic coordination environment is also shown to consist of ion aggregates involving two anions coordinated with Li^+, denoted Anion/Li^+ (red, Figure 5b and Table S5).

These analyses suggest that in PEO, as the lithium salts are completely dissociated, supported by the MD snapshots in Figure 6a−c, Li^+ speciation remains the same, and anion speciation changes from predominantly noninteracting Anion/Anion for LiTFSI/PEO and LiDFTFSI/PEO to Anion/Polymer for LiDFSI/PEO. However, as the lithium salts undergo partial dissociation in PCL, as shown in Figure 6d−f, when the anion is coordinated to both Li^+ and the PCL polymer matrix as Anion/Polymer/Li^+, a synergy occurs: the anion mobility is restricted as the anion is coordinated to both the CL units from PCL, and the Li^+ ions, while the Li^+ ions can move even more freely due to the weaker Li salt dissociation in PCL than if Li^+ ions were only coordinated to either one of the two components individually.

Importantly, when compared to PEO, the anionic mobility is significantly more restricted in the PCL host matrix, which is experimentally observed, as lower σ_{total} is observed in PCL-based SPEs. The speciation and charge carriers differ significantly in both polymers, with PCL-SPEs exhibiting polymer−anion assisted Li^+ polymer chain coordination, whereas in PEO-SPEs, Li^+ coordinated solely to EO units is observed, as reported in the literature.[11,12,24] Hence, a decrease in σ_{total} is observed for PCL-based SPEs compared to PEO-based SPEs, however, with the benefit of a higher t_{Li^+} for the former system.

4. CONCLUSION

In conclusion, SPEs are complex mixtures, with their electrochemical properties influenced by ion−ion and ion−polymer interactions as well as charge carrier speciation. By systematically substituting F atoms by H in LiTFSI salts as a case study, we show how additional noncovalent weak hydrogen bond interactions in PEO-based SPEs can be exploited to tune the σ_{total} and t_{Li^+} of the resulting electrolyte. By also modifying the polymer host (substituting PEO by PCL) to induce different Li^+ and anion coordination environments as well as charge carrier speciation, we demonstrate that an even deeper control of these properties can be practically achieved. These insights, emerging from both experimental and theoretical studies, are useful to better understand these complex functional materials and guide SPE discovery—for example, by adjusting the amount of H substitution in the anions, looking for alternative chemical modifications that can hinder anion mobility through specific interaction with the polymer host, and polymers that optimize those interactions and promote the desired speciation.

■ ASSOCIATED CONTENT

Supporting Information

The Supporting Information is available free of charge at https://pubs.acs.org/doi/10.1021/acs.jpcc.2c07032.

Supporting tables and figures from DSC, EIS, and MD simulations for the different investigated systems (PDF)

■ AUTHOR INFORMATION

Corresponding Authors

Javier Carrasco − *Centre for Cooperative Research on Alternative Energies (CIC energiGUNE), Basque Research and Technology Alliance (BRTA), 01510 Vitoria-Gasteiz, Spain*; orcid.org/0000-0003-3117-6933; Email: jcarrasco@cicenergigune.com

María Martínez-Ibañez − *Centre for Cooperative Research on Alternative Energies (CIC energiGUNE), Basque Research and Technology Alliance (BRTA), 01510 Vitoria-Gasteiz, Spain*; Email: mmartinez@cicenergigune.com

Authors

Brigette A. Fortuin − *Centre for Cooperative Research on Alternative Energies (CIC energiGUNE), Basque Research and Technology Alliance (BRTA), 01510 Vitoria-Gasteiz, Spain; Department of Physics, University of the Basque Country (UPV/EHU), 48940 Leioa, Spain*; orcid.org/0000-0003-3592-9365

Leire Meabe − *Centre for Cooperative Research on Alternative Energies (CIC energiGUNE), Basque Research and Technology Alliance (BRTA), 01510 Vitoria-Gasteiz, Spain*

Sergio Rodriguez Peña − *Centre for Cooperative Research on Alternative Energies (CIC energiGUNE), Basque Research and Technology Alliance (BRTA), 01510 Vitoria-Gasteiz, Spain; Department of Physics, University of the Basque Country (UPV/EHU), 48940 Leioa, Spain*

Yan Zhang − *Centre for Cooperative Research on Alternative Energies (CIC energiGUNE), Basque Research and Technology Alliance (BRTA), 01510 Vitoria-Gasteiz, Spain*

Lixin Qiao − *Centre for Cooperative Research on Alternative Energies (CIC energiGUNE), Basque Research and Technology Alliance (BRTA), 01510 Vitoria-Gasteiz, Spain*; orcid.org/0000-0003-1892-5477

Julen Etxabe − *Centre for Cooperative Research on Alternative Energies (CIC energiGUNE), Basque Research and Technology Alliance (BRTA), 01510 Vitoria-Gasteiz, Spain*

Lorena Garcia − *Centre for Cooperative Research on Alternative Energies (CIC energiGUNE), Basque Research and Technology Alliance (BRTA), 01510 Vitoria-Gasteiz, Spain*

Hegoi Manzano − *Department of Physics, University of the Basque Country (UPV/EHU), 48940 Leioa, Spain*; orcid.org/0000-0001-7992-2718

Michel Armand − *Centre for Cooperative Research on Alternative Energies (CIC energiGUNE), Basque Research and Technology Alliance (BRTA), 01510 Vitoria-Gasteiz, Spain*; orcid.org/0000-0002-1303-9233

Complete contact information is available at: https://pubs.acs.org/10.1021/acs.jpcc.2c07032

Notes

The authors declare no competing financial interest.

■ ACKNOWLEDGMENTS

The authors acknowledge support from the European Commission grant for Erasmus Mundus Joint Master's Degree MESC+ under Framework Agreement Number 2018-1424/001-001-EMJMD, the EU Marie Sklodowska-Curie COFUND DESTINY project under Grant Agreement No. 945357, and the Basque Government PhD Grant. H.M. acknowledges funding from the "Departamento de Educación, Política Lingüística y Cultura del Gobierno Vasco" (Grant IT1358-22). They also thank SGI/IZO-SGIker UPV/EHU for supercomputing resources.

■ REFERENCES

(1) Yang, G.; Chanthad, C.; Oh, H.; Ayhan, I. A.; Wang, Q. Organic-Inorganic Hybrid Electrolytes from Ionic Liquid-Functionalized Octasilsesquioxane for Lithium Metal Batteries. *J. Mater. Chem. A Mater.* **2017**, *5* (34), 18012−18019.
(2) Wang, X.; Kerr, R.; Chen, F.; Goujon, N.; Pringle, J. M.; Mecerreyes, D.; Forsyth, M.; Howlett, P. C. Toward High-Energy-Density Lithium Metal Batteries: Opportunities and Challenges for Solid Organic Electrolytes. *Adv. Mater.* **2020**, *32*, 1905219.
(3) Liu, B.; Zhang, J. G.; Xu, W. Advancing Lithium Metal Batteries. *Joule.* **2018**, *2*, 833−845.
(4) Korthauer, R.*Lithium-Ion Batteries: Basics and Applications*; Springer: Berlin, 2018.
(5) Varzi, A.; Raccichini, R.; Passerini, S.; Scrosati, B. Challenges and Prospects of the Role of Solid Electrolytes in the Revitalization of Lithium Metal Batteries. *J. Mater. Chem. A Mater.* **2016**, *4* (44), 17251−17259.
(6) Zhu, J.; Zhang, Z.; Zhao, S.; Westover, A. S.; Belharouak, I.; Cao, P. F. Single-Ion Conducting Polymer Electrolytes for Solid-State Lithium-Metal Batteries: Design, Performance, and Challenges. *Advanced Energy Materials.* **2021**, *11*, 2003836.
(7) Rollo-Walker, G.; Malic, N.; Wang, X.; Chiefari, J.; Forsyth, M. Development and Progression of Polymer Electrolytes for Batteries: Influence of Structure and Chemistry. *Polymers.* **2021**, *13*, 4127.
(8) Zhang, H.; Chen, F.; Carrasco, J. Nanoscale Modelling of Polymer Electrolytes for Rechargeable Batteries. *Energy Storage Materials.* **2021**, *36*, 77−90.
(9) Li, J.; Kong, Z.; Liu, X.; Zheng, B.; Fan, Q. H.; Garratt, E.; Schuelke, T.; Wang, K.; Xu, H.; Jin, H. Strategies to Anode Protection in Lithium Metal Battery: A Review. *InfoMater.* **2021**, *3* (12), 1333−1363.
(10) Wright, P. v. Electrical Conductivity in Ionic Complexes of Poly(Ethylene Oxide). *Polym. Int.* **1975**, *7* (5), 319−327.
(11) Qiao, L.; Oteo, U.; Zhang, Y.; Peña, S. R.; Martínez-Ibañez, M.; Santiago, A.; Cid, R.; Meabe, L.; Manzano, H.; Carrasco, J.; Zhang, H.; Armand, M. Trifluoromethyl-Free Anion for Highly Stable Lithium Metal Polymer Batteries. *Energy Storage Mater.* **2020**, *32*, 225−233.
(12) Meabe, L.; Peña, S. R.; Martinez-Ibañez, M.; Zhang, Y.; Lobato, E.; Manzano, H.; Armand, M.; Carrasco, J.; Zhang, H. Insight into the Ionic Transport of Solid Polymer Electrolytes in Polyether and Polyester Blends. *J. Phys. Chem. C* **2020**, *124* (33), 17981−17991.
(13) Edman, L.; Doeff, M. M.; Ferry, A.; Kerr, J.; de Jonghe, L. C. Transport Properties of the Solid Polymer Electrolyte System $P(EO)_nLiTFSI$. *J. Phys. Chem. B* **2000**, *104* (15), 3476−3480.
(14) Andersson, R.; Hernández, G.; Mindemark, J. Quantifying the Ion Coordination Strength in Polymer Electrolytes. *Phys. Chem. Chem. Phys.* **2022**, *24* (26), 16343−16352.
(15) Xue, Z.; He, D.; Xie, X. Poly(Ethylene Oxide)-Based Electrolytes for Lithium-Ion Batteries. *J. Mater. Chem. A* **2015**, *3*, 19218−19253.
(16) Rosenwinkel, M. P.; Andersson, R.; Mindemark, J.; Schönhoff, M. Coordination Effects in Polymer Electrolytes: Fast Li^+ Transport by Weak Ion Binding. *J. Phys. Chem. C* **2020**, *124* (43), 23588−23596.
(17) Eriksson, T.; Mace, A.; Mindemark, J.; Brandell, D. The Role of Coordination Strength in Solid Polymer Electrolytes: Compositional Dependence of Transference Numbers in the Poly(ε-Caprolactone)-Poly(Trimethylene Carbonate) System. *Phys. Chem. Chem. Phys.* **2021**, *23* (45), 25550−25557.
(18) Bergfelt, A.; Lacey, M. J.; Hedman, J.; Sångeland, C.; Brandell, D.; Bowden, T. ε-Caprolactone-Based Solid Polymer Electrolytes for Lithium-Ion Batteries: Synthesis, Electrochemical Characterization and Mechanical Stabilization by Block Copolymerization. *RSC Adv.* **2018**, *8* (30), 16716−16725.
(19) Sångeland, C.; Tjessem, T.; Mindemark, J.; Brandell, D. Overcoming the Obstacle of Polymer-Polymer Resistances in Double Layer Solid Polymer Electrolytes. *Journal of Physical Chemistry Letters.* **2021**, *12* (11), 2809−2814.
(20) Rey, I.; Lassègues, J. C.; Grondin, J.; Servant, L. Infrared and Raman Study of the PEO-LiTFSI Polymer Electrolyte. *Electrochim. Acta* **1998**, *43* (10−11), 1505−1510.
(21) Lassègues, J. C.; Grondin, J.; Aupetit, C.; Johansson, P. Spectroscopic Identification of the Lithium Ion Transporting Species in LiTFSI-Doped Ionic Liquids. *J. Phys. Chem. A* **2009**, *113* (1), 305−314.
(22) Marzantowicz, M.; Dygas, J. R.; Krok, F.; Florjańczyk, Z.; Zygadło-Monikowska, E. Influence of Crystalline Complexes on Electrical Properties of PEO:LiTFSI Electrolyte. *Electrochim. Acta* **2007**, *53* (4), 1518−1526.
(23) Zhang, H.; Oteo, U.; Judez, X.; Eshetu, G. G.; Martinez-Ibañez, M.; Carrasco, J.; Li, C.; Armand, M. Designer Anion Enabling Solid-State Lithium-Sulfur Batteries. *Joule.* **2019**, *3* (7), 1689−1702.
(24) Oteo, U.; Martinez-Ibañez, M.; Aldalur, I.; Sanchez-Diez, E.; Carrasco, J.; Armand, M.; Zhang, H. Improvement of the Cationic Transport in Polymer Electrolytes with (Difluoromethanesulfonyl)-(Trifluoromethanesulfonyl) Imide Salts. *ChemElectroChem.* **2019**, *6* (4), 1019−1022.
(25) Santiago, A.; Castillo, J.; Garbayo, I.; Saenz De Buruaga, A.; Coca Clemente, J. A.; Qiao, L.; Cid Barreno, R.; Martinez-Ibañez, M.; Armand, M.; Zhang, H.; Li, C. Salt Additives for Improving Cyclability of Polymer-Based All-Solid-State Lithium-Sulfur Batteries. *ACS Appl. Energy Mater.* **2021**, *4* (5), 4459−4464.
(26) Maurel, A.; Armand, M.; Grugeon, S.; Fleutot, B.; Davoisne, C.; Tortajada, H.; Courty, M.; Panier, S.; Dupont, L. Poly(Ethylene Oxide)-LiTFSI Solid Polymer Electrolyte Filaments for Fused Deposition Modeling Three-Dimensional Printing. *J. Electrochem. Soc.* **2020**, *167* (7), 070536.
(27) Mindemark, J.; Sun, B.; Törmä, E.; Brandell, D. High-Performance Solid Polymer Electrolytes for Lithium Batteries Operational at Ambient Temperature. *J. Power Sources.* **2015**, *298*, 166−170.
(28) Loaiza, L. C.; Johansson, P. Li-Salt Doped Single-Ion Conducting Polymer Electrolytes for Lithium Battery Application. *Macromol. Chem. Phys.* **2022**, *223* (8), 2100419−2100427.
(29) Jalbert, P.-M.; Commarieu, B.; Daigle, J.-C.; Claverie, J. P.; Zaghib, K. A 3D Network Based on Poly(ε-Caprolactone) Macromonomers as Polymer Electrolyte for Solid State Lithium Metal Batteries. *J. Electrochem. Soc.* **2020**, *167* (8), 080527.
(30) Zhang, H.; Oteo, U.; Zhu, H.; Judez, X.; Martinez-Ibañez, M.; Aldalur, I.; Sanchez-Diez, E.; Li, C.; Carrasco, J.; Forsyth, M.; Armand, M. Enhanced Lithium-Ion Conductivity of Polymer Electrolytes by Selective Introduction of Hydrogen into the Anion. *Angewandte Chemie - International Edition.* **2019**, *58* (23), 7829−7834.
(31) Suo, L.; Hu, Y. S.; Li, H.; Armand, M.; Chen, L. A New Class of Solvent-in-Salt Electrolyte for High-Energy Rechargeable Metallic Lithium Batteries. *Nat. Commun.* **2013**, *4*, 4.
(32) Pronk, S.; Páll, S.; Schulz, R.; Larsson, P.; Bjelkmar, P.; Apostolov, R.; Shirts, M. R.; Smith, J. C.; Kasson, P. M.; van der Spoel, D.; Hess, B.; Lindahl, E. GROMACS 4.5: A High-Throughput and Highly Parallel Open-Source Molecular Simulation Toolkit. *Bioinformatics.* **2013**, *29* (7), 845−854.
(33) Kaminski, G. A.; Friesner, R. A.; Tirado-Rives, J.; Jorgensen, W. L. Evaluation and Reparametrization of the OPLS-AA Force Field for

https://doi.org/10.1021/acs.jpcc.2c07032
J. Phys. Chem. C 2023, 127, 1955−1964

Proteins via Comparison with Accurate Quantum Chemical Calculations on Peptides. *J. Phys. Chem. B* **2001**, *105* (28), 6474−6487.
(34) Jorgensen, W. L.; Maxwell, D. S.; Tirado-Rives, J. Development and Testing of the OPLS All-Atom Force Field on Conformational Energetics and Properties of Organic Liquids. *J. Am. Chem. Soc.* **1996**, *118* (45), 11225−11236.
(35) Mcdonald, N. A.; Jorgensen, W. L. Development of an All-Atom Force Field for Heterocycles. Properties of Liquid Pyrrole, Furan, Diazoles, and Oxazoles. *J. Mol. Structure: THEOCHEM.* **1998**, *424* (1−2), 145−155.
(36) Price, M. L. P.; Ostrovsky, D.; Jorgensen, W. L. Gas-Phase and Liquid-State Properties of Esters, Nitriles, and Nitro Compounds with the OPLS-AA Force Field. *Computational Chemistry.* **2001**, *22* (13), 1340−1352.
(37) Rizzo, R. C.; Jorgensen, W. L. OPLS All-Atom Model for Amines: Resolution of the Amine Hydration Problem. *J. Am. Chem. Soc.* **1999**, *121* (20), 4827−4836.
(38) Watkins, E. K.; Jorgensen, W. L. Perfluoroalkanes: Conformational Analysis and Liquid-State Properties from Ab Initio and Monte Carlo Calculations. *J. Phys. Chem. A* **2001**, *105* (16), 4118−4125.
(39) Havu, V.; Blum, V.; Havu, P.; Scheffler, M. Efficient O (N) Integration for All-Electron Electronic Structure Calculation Using Numeric Basis Functions. *J. Comput. Phys.* **2009**, *228* (22), 8367−8379.
(40) Blum, V.; Gehrke, R.; Hanke, F.; Havu, P.; Havu, V.; Ren, X.; Reuter, K.; Scheffler, M. Ab Initio Molecular Simulations with Numeric Atom-Centered Orbitals. *Comput. Phys. Commun.* **2009**, *180* (11), 2175−2196.
(41) Lee, C.; Yang, W.; Parr, R. G. Development of the Colic-Salvetti Correlation-Energy Formula into a Functional of the Electron Density. *Phys. Rev. B Condens Matter.* **1988**, *37* (2), 785−789.
(42) Becke, A. D. Density-functional thermochemistry. III. The role of exact exchange. *J. Chem. Phys.* **1993**, *98* (7), 5648−5652.
(43) Molinari, N.; Mailoa, J. P.; Kozinsky, B. Effect of High Salt Concentration on Ion Clustering and Transport in Polymer Solid Electrolytes: A Molecular Dynamics Study of PEO-LiTFSI. *Chem. Mater.* **2018**, *30* (18), 6298−6306.
(44) Gudla, H.; Zhang, C.; Brandell, D. Effects of Solvent Polarity on Li-Ion Diffusion in Polymer Electrolytes: An All-Atom Molecular Dynamics Study with Charge Scaling. *J. Phys. Chem. B* **2020**, *124* (37), 8124−8131.
(45) Brooks, D. J.; Merinov, B. v.; Goddard, W. A.; Kozinsky, B.; Mailoa, J. Atomistic Description of Ionic Diffusion in PEO-LiTFSI: Effect of Temperature, Molecular Weight, and Ionic Concentration. *Macromolecules.* **2018**, *51* (21), 8987−8995.
(46) Kang, P.; Wu, L.; Chen, D.; Su, Y.; Zhu, Y.; Lan, J.; Yang, X.; Sui, G. Dynamical Ion Association and Transport Properties in PEO-LiTFSI Electrolytes: Effect of Salt Concentration. *J. Phys. Chem. B* **2022**, *126* (24), 4531−4542.
(47) Mabuchi, T.; Nakajima, K.; Tokumasu, T. Molecular Dynamics Study of Ion Transport in Polymer Electrolytes of All-Solid-State Li-Ion Batteries. *Micromachines (Basel).* **2021**, *12* (9), 1012.
(48) Zhang, H.; Chen, F.; Lakuntza, O.; Oteo, U.; Qiao, L.; Martinez-Ibañez, M.; Zhu, H.; Carrasco, J.; Forsyth, M.; Armand, M. Suppressed Mobility of Negative Charges in Polymer Electrolytes with an Ether-Functionalized Anion. *Angew. Chem.* **2019**, *131* (35), 12198−12203.
(49) Armand, M. B. Polymer Electrolytes. *Annu. Rev. Mater. Sci.* **1986**, *16*, 245−261.
(50) Edman, L. Ion Association and Ion Solvation Effects at the Crystalline-Amorphous Phase Transition in PEO-LiTFSI. *J. Phys. Chem. B* **2000**, *104* (31), 7254−7258.
(51) Capiglia, C.; Imanishi, N.; Takeda, Y.; Henderson, W. A.; Passerini, S. Poly(Ethylene Oxide) $LiN(SO_2CF_2CF_3)_2$ Polymer Electrolytes. *J. Electrochem. Soc.* **2003**, *150* (4), A525.

https://doi.org/10.1021/acs.jpcc.2c07032
J. Phys. Chem. C 2023, 127, 1955−1964